J. Eur. Opt. Society-Rapid Publ. 2023, **19**, 11

https://doi.org/10.1051/jeos/2023007
Available online at: https://jeos.edpsciences.org

Journal of the European Optical Society-Rapid Publications

RESEARCH ARTICLE OPEN ACCESS

Monitoring and meaning of vibrations in robot polishing

Max Schneckenburger[1,2,a,*], Rui Almeida[1,a], Sven Höfler[1,3,a], Ines Braga[4], and Rainer Börret[1]

[1] Hochschule Aalen, Centre for Optical Technologies, Aalen BW 73430, Germany
[2] Technische Universität Ilmenau, Ilmenau TH 98693, Germany
[3] Glasgow Caledonian University, Scotland G4 OBA, United Kingdom
[4] University of Minho, Braga 4704-553, Portugal

Received 5 December 2021 / Accepted 10 February 2023

Abstract. Robot polishing is increasingly used in the production of high-end glass work pieces such as astronomy mirrors, lithography lenses, laser gyroscopes or high-precision coordinate measuring machines. The quality of optical components such as lenses or mirrors can be described by shape errors and surface roughness. Whilst the trend towards sub nanometre level surfaces finishes and features progresses, matching both form and finish coherently in complex parts remains a major challenge. With larger or more precise optics, the influence of process instabilities on the quality of the optics to be polished has a greater impact. Vibrations at a polishing head have a negative influence on the polishing result. These vibrations are caused by bearing damage, motors and other excitations (e.g. gears, belts). The aim of this work is the determination of vibrations at a polishing head and their avoidance strategies. Different bearing conditions are considered: new and perfect bearing, a bearing that has been in contact with polish (rust) and a bearing with repeatable damage (groove milled on the running surface). It can be shown that the frequencies of bearings affect the polishing tool. Furthermore, reasons for and against vibrations in the process are discussed. For the case of vibrationless machining, avoidance strategies were presented.

Keywords: Polishing, Robot, Vibration measurements, Condition monitoring, Bearing damage.

Abbreviation

ABB	Asea Brown Boveri (a Swiss company)
AVC	Active Vibration Controlling
BPFFI	Ball Pass Frequency Factor Inner
BPFFO	Ball Pass Frequency Factor Outer
BSFF	Ball Spin Frequency Factor
CCP	Computer Controlled Polishing
CMP	Chemical Mechanical Polishing
EUV	Extreme Ultra Violet
FFT	Fast Fourier Transformation
FTFFI	Fundamental Train Frequency Factor Inner
FTFFO	Fundamental Train Frequency Factor Outer
IRB	Industrial Robot
PLC	Programmable Logic Controller
PV	Peak-to-Valley
RMS	Root Mean Squared
RPFFB	Ring Pass Frequency Factor on Rolling Element

The present work combines the key technologies of the 21st century "Optical Technologies", "Condition-monitoring" and "Sensor use for 100% control" with the objective of contributing to an increase in the understanding of polishing process of optical surfaces and for process control. The experimental and theoretical investigations carried out within the framework of this work on the mechanisms of action of the process, as well as on the technological interrelationships of the influencing parameters for vibrations, are intended to provide further fundamentals for the robotic polishing of glass. Special attention is paid to the application of condition monitoring to the largely empirical process technology of glass polishing. On one hand, the use of sensors serves as business motivation such as plannable maintenance measures, shortening of downtimes, cost minimisation, especially predictive maintenance and condition monitoring. On the other hand, the sensors and actuators can be used to make scientific statements and achieve repeatable results, including the observation of new effects that remain hidden due to process divergence

* Corresponding author: max.schneckenburger@asml.com
[a] All three main authors have driven this work in equal parts; their order does not give any information about possible additional work.

and improvements can be made on recognized weak spots of the process. The use of sensors also provides the basis for readjusting the process parameters in the event of damage or for intervention by the machine operator.

1 Introduction

Today, polishing is still a very skilled process based mainly on experience and empiricism. Due to its complexity, the mechanism of action of the process is still not fully understood today [1–7]. Compared to other ablative processes, such as grinding and milling [8], the influence of machine dynamics in polishing has been insufficiently scientifically investigated.

According to the "Steering Committee Optical Technologies" (original: Lenkungskreis Optische Technologien), process control in polishing is a challenge for the 21st century. Due to the large number of process-relevant influencing variables, process control is difficult. The Steering Committee recommends, at least for preferred glasses, the investigation of the parameters, the monitoring of the polishing agent, as well as the integration of sensors and measuring technology for online surface assessment [9]. The American counterpart "Harnessing Light" describes Computer Controlled Polishing (CCP) and the production of high-precision optics, for example for EUV technology (extreme ultraviolet radiation), as one of the key technologies of the 21st century. Here, roughnesses of 0.1 nm rms and 1 nm Peak-to-Valley (PV) are achieved [10]. For sustained repeatability, the performance of the manufacturing processes must be increased [11].

The main component of the polishing process consists of a polishing tool that is passed over the glass surface. All material removal takes place in the polishing gap, the area between the polishing tool and the glass surface. The polishing tool usually consists of an elastomer and a polishing film, the viscoelastic polishing agent carrier. Due to the elastic behaviour of the material, the polishing tool clings to the glass surface, even if it is uneven. The polishing gap usually contains a polishing suspension of water and polishing grains: the amount of polishing grains in the gap determines the process, both for roughness and for material removal [12]. Process vibrations lead to a pump-like effect, resulting in an increased polish feed in the gap. In addition, vibrations lead to higher local temperature input and greater process fluctuation of the normal force. Contact between the polishing tool and the workpiece can also occur: Ideally, both should only touch the polishing grains. "Very slow and vibrationless speeds" are recommended for high quality surfaces with less roughness [13]. Accordingly, controlled vibration support is recommended to maximise material removal. Due to the structure of moving elements, every optical production machine has frequencies and vibrations. Due to different construction types and manufacturing tolerances, these are individual for each machine. Similar frequencies are calculated for similar machines in the Fast Fourier Transformation (FFT).

The objectives of this work are to strengthen the process understanding, the wear detection on the polishing head and the generation of better workpiece surfaces. Wear detection enables a maintenance plan, prediction of process variations and failure. Rolling bearings are widely used standard components in the mechanical implementation of rotating machinery. If one element of the bearing is damaged and comes into contact with another element of the bearing, an impact force is generated which leads to an impulsive reaction of the bearing. A defect on one of the elements transmits vibrations to all other rolling bearing components. Therefore, a vibration analysis of the process is useful for condition monitoring in order to detect damage and failures on the polishing head at an early stage [14]. Vibration spectrum analysis is a popular technique alongside others such as time domain and time-frequency domain for tracking machine operating conditions. There are already some publications in condition monitoring by accelerators [15–17].

The wear of the components and the bearings has an influence on the vibrations in the process. In polishing, the damage types that primarily occur are washing out of the bearing grease, rust, wear, increased wear, and additional wear caused by polishing agents. In this paper, damage on the bearing outer ring, rust and a bearing without lubrication are compared. Especially a rusting bearing has an influence on the polishing process: Rust Fe_2O_3, also known as »polishing red« is used in polishing as an independent polishing agent. If SiO_2 recondenses on the glass during the polishing process, iron particles can be enclosed. This happens with all polishing grains and is a conventional process and is an explanation for the smoothing in the polishing process. In laser optics, these iron particles heat up more than the glass itself and thermal stress cracks occur. Therefore, it is recommended not to use polishing red for laser optics [18].

Vibrations are used strategically during grinding or polishing, for example, with ultra-sonic. Akbari investigated the ultrasonic vibration effects on grinding process of aluminum ceramic. The surface roughness get improved by 8% and the grinding forces up to 22% [19]. Jianhua reduced the normal grinding forces on SiO_2 up to 65.6% and a larger feed rate could be adopted, which leads to material removal rate and machining efficiency [20]. For a number of optical materials, a higher material removal rate and a better surface quality, i.e. lower sub-surface damages, could be achieved [21]. This results from the superposition of the oscillating amplitude with the rotation of the tool. The total grinding/polishing speed can be calculated by using the following equation with the cutting velocity v_c, the cutting velocity by ultrasonic tool oscillation v_{cUS}, the tool diameter d, the rotational speed n, the amplitude of ultrasonic oscillation X_{max} and the frequency f [22]:

$$v_{cGES} = \sqrt{v_c^2 + v_{cUS}^2} = \sqrt{\left(\frac{\pi \cdot d \cdot n}{60.000}\right)^2 + (4X_{max}f)^2} \quad (1)$$

The ultrasonic support has mainly a positive effect for small to medium sized tool geometries and higher rotational speeds. By reducing the process forces, lower stresses are introduced, which means less sub-surface damage in the glass surface [20, 23].

In the literature, there are already initial publications on primarily unwanted vibrations in glass polishing: Slow and »vibrationless« speeds are the requirements placed on machines for the production of high-precision surfaces by polishing [13]. In contrast to the process vibrations in glass polishing (<10 nm [12]), frequencies with amplitudes of several hundred nanometres up to 40 µm occur in ultrasonic assisted polishing [24, 25]. Possible consequences for vibrations during the polishing process are a better supply of polishing slurry, larger loads and higher local temperature increases due to the dissipation of vibration energy. In addition, there is intermitted contact between the polishing tool and the glass surface due to strong vibrations. Due to theoretically possible large amplitudes of vibrations, pressure distributions can occur on the work piece surface. Machines with greater vibration amplitudes induced higher material removal due to enhanced localized micro pumping to the slurry. On the other side are higher surface roughness values caused by macro scale intermitted work piece tool contact [12].

Many parallels can be found between the polishing of optical surfaces and the chemical-mechanical planarisation of wafers, especially in the area of material removal hypotheses. In Chemical Mechanical Polishing (CMP), also called chemical mechanical planarisation, wafers of different materials (including monocrystalline silicon or silicon carbide) are polished to a thickness accuracy of ± 0.5 µm [26]. By planarising, multi-layer microelectrical circuits can be realised on wafers. Due to the higher economic importance and the larger research community, there are a larger number of publications for chemical-mechanical planarising than for glass polishing. This polishing process differs from the glass polishing process in geometry (exclusively planar workpieces), workpiece size (a workpiece contour), relative speed, the movement system and the number of pieces. CMP of wafers is understood to be similar to the polishing of glass workpieces and is primarily heuristic, i.e. researched via trial and error [27]. As long as the process can be held constant, the removal prediction is accurate. If parameters are changed in the process, no detailed statement about the process can be made [28]. Another reason for the low understanding in CMP is also the low use of in situ sensors [29]. Accelerators are used in CMP wafer polishing for condition monitoring and predictive maintenance. Currently, the condition of the polishing pad and the failure of individual polishing slurry nozzles can be determined predictively. Machine learning algorithms and big data analyses are used in the evaluation. These sensors are also used in the robot handling of wafers. This detects whether the robot indirectly damages the wafer due to incorrect handling [30].

The bearings provide relative positioning and rotational freedom, usually transferring a load between the shaft and housing. The geometry of such a rolling bearing, which consists of an outer and an inner ring, as well as the rolling elements and a cage, is shown in Figure 1. The latter positions the rolling elements at an even distance around the inner ring. Tolerances and damages of the rolling bearing generate a periodically occurring series of impacts, which are known as bearing frequencies.

A total of four frequencies are usually distinguished; six frequencies are given on commercial websites. These result from the relative movements ($\vec{v}_{\mathrm{rel}}$) of the individual ball bearing components outer ring, inner ring, rolling elements and cage. Due to the respective distance from the axis of rotation, the ball bearing inner ring, the ball bearing outer ring, the respective balls and the cage each have a different rotational speed. The frequencies depend on only three factors: the rolling element diameter, their running diameter and their number. For the frequencies, it is assumed that only one ring is moved and the other remains static. The rolling elements roll on the outer ring and provide the *Ball Pass Frequency Factor Outer* (*BPFFO*) or the *Ball Pass Frequency Factor Inner* (*BPFFI*) on the inner ring. The third important frequency is the *Ball Spin Frequency Factor* (*BSFF*), which is the rotational speed of the respective rolling elements around their own axis of rotation. As the rolling element rolls on both the inner and outer ring, the frequency *Ring Pass Frequency Factor on Rolling Element* (*RPFFB*) is generated, which has twice the value of *BSFF*. The frequency of the cage with respect to the inner ring is called *Fundamental Train Frequency Factor Inner* (*FTFFI*) and to the outer ring *Fundamental Train Frequency Factor Outer* (*FTFFO*). The cage frequency will almost always fall between 35% and 45% of the bearing inner ring rotational speed. *FTFFI* and *FTFFO* together give the value 1 and the addition of *BPFFO* and *BPFFI* gives the number of rolling elements in the bearing. The frequency values are calculated as follows and can be derived via the respective relative velocity:

Ball Pass Frequency Factor Outer [31] (2):

$$\mathrm{BPFFO}\left[\frac{1}{s}\right] = \frac{n}{2}\left(1 - \frac{d_{\mathrm{Ball}}}{d_{\mathrm{Pitch}}}\right); \tag{2}$$

Ball Pass Frequency Factor Inner [31] (3):

$$\mathrm{BPFFI}\left[\frac{1}{s}\right] = \frac{n}{2}\left(1 + \frac{d_{\mathrm{Ball}}}{d_{\mathrm{Pitch}}}\right); \tag{3}$$

Ball Spin Frequency Factor [32] (4):

$$\mathrm{BSFF}\left[\frac{1}{s}\right] = \frac{d_{\mathrm{Pitch}}}{2 * d_{\mathrm{Ball}}}\left(1 - \left(\frac{d_{\mathrm{Ball}}}{d_{\mathrm{Pitch}}}\right)^2\right); \tag{4}$$

Ring Pass Frequency Factor on Rolling Element [33] (5):

$$\mathrm{RPFFB}\left[\frac{1}{s}\right] = \frac{d_{\mathrm{Pitch}}}{d_{\mathrm{Ball}}}\left(1 - \left(\frac{d_{\mathrm{Ball}}}{d_{\mathrm{Pitch}}}\right)^2\right) = 2 * \mathrm{BSFF}; \tag{5}$$

Fundamental Train Frequency Factor Inner [32] (6):

$$\mathrm{FTFFI}\left[\frac{1}{s}\right] = \frac{1}{2}\left(1 - \frac{d_{\mathrm{Ball}}}{d_{\mathrm{Pitch}}}\right); \tag{6}$$

Fundamental Train Frequency Factor Outer [33] (7):

$$\mathrm{FTFFO}\left[\frac{1}{s}\right] = \frac{1}{2}\left(1 + \frac{d_{\mathrm{Ball}}}{d_{\mathrm{Pitch}}}\right) = 1 - \mathrm{FTFFI}, \tag{7}$$

n: number of rolling elements.

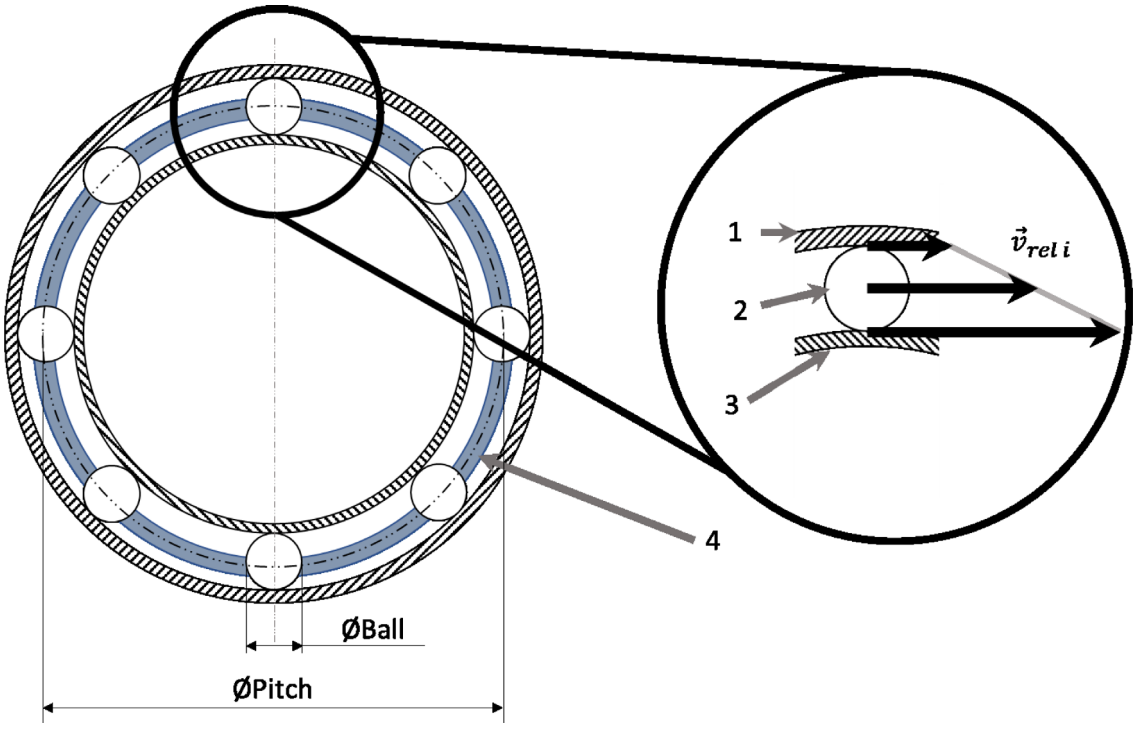

Figure 1. Schematic image of a bearing. Legend: 1 – Outer ring; 2 – Rolling element; 3 – Inner ring; 4 – Cage; Black arrow: velocity vector of each element, the outer ring (smallest arrow) is static ($v = 0$).

2 Proceeding

This section deals with the general basics of this work. The individual steps that are necessary for data acquisition are shown. These include the process overview, the measurement technology and the experimental design. In addition, the selection of sensors and the set up are discussed.

The motion system for this research project is an Industrial Robot ABB IRB 4400 with an S4C+ controller. A polishing head is attached to the robot, which has a rotation motor for the rotary movement and a linear drive (pneumatic or electric) for the z-stroke. The polishing tool consists of a workpiece carrier, an elastomer for height compensation and the polishing pad. The robot cell is enclosed in a protective cage. The polishing tray collects the polishing agent and feeds it back into the polishing agent reservoir. A peristaltic pump returns the polishing suspension to the polishing head and supplies the process with new polishing agent. The polishing suspension filters dirt particles before the nozzle on the polishing head and before the reservoir. The set-up is shown schematically in Figure 2.

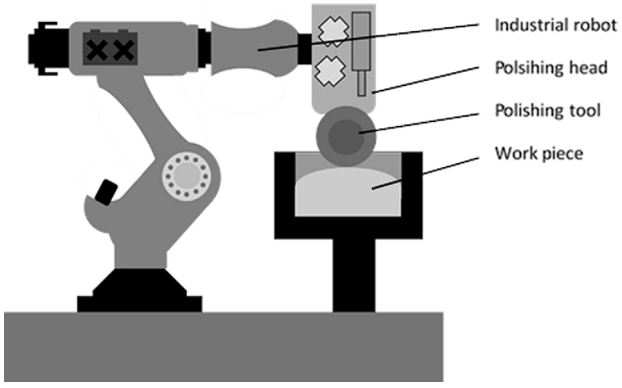

Figure 2. Schematic illustration of the robot polishing cell.

2.1 Polishing head

Figure 3 shows the section view of a polishing head, the core of the setup. A conventional polishing head usually consists of a rotational and a vertical axis. To achieve this, a polishing head consists of a number of bearings, each of which excites frequencies. The illustration shows the attachment of the polishing tool and the attachment of the vibration sensor. This setup is representative for comparable applications or machines. In principle, the bearing types can be exchanged and/or scaled.

The bearing that is mainly considered is the bearing closest to the polishing tool, the S6001. This is the one most likely to come into contact with polishing medium and has the greatest influence on the running properties and polishing result. A polishing head usually consists of a rotation axis to realise the typical rotary movement and a vertical axis that regulates the contact pressure. Two different sensors are used in the experiments: an intelligent sensor that can be connected to the PLC via IO-Link and one that is inexpensive and almost self-taught in its handling.

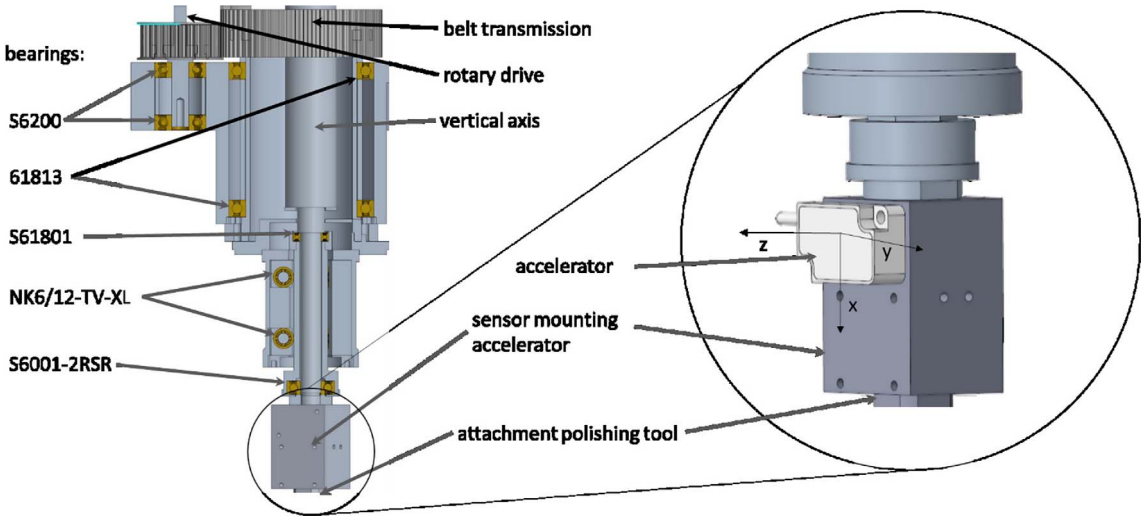

Figure 3. Sectional view of a robot polishing head with vibration sensor attachment and all ball bearings and damaged.

Figure 4. Left: new bearing, middle: bearing with milled structure and on the right handside a rusty bearing without grease.

An integrated acceleration sensor is used as the second sensor. Both are dealt with in detail in a later subchapter. Both sensors can be attached to the adapters for the polishing head as well as to the adapters of the test stand presented later. The effective zone of the respective sensor is always directly above the centre of the bearing.

Figure 4 shows the three 6001 test bearings: one new (similar to the bearing later used with already approximately 50 h running time), one with milling damage and one that is rusty and grease-free due to polishing slurry. The new bearing and the bearing with already 50 h running time are visually indistinguishable from each other. The milling damage is only on the outer ring and has been repeatedly inserted into the bearing. These three shown or four later used ball bearings represent the different bearing conditions: factory new, worn in, rusted (e.g. by polishing suspension).

The frequencies are calculated according to the formulas (2)–(7) and can also be calculated automatically on the website of the respective bearing manufacturer and the frequencies are shown in Table 1.

2.2 Test rig

As there are many damping elements in a polishing head, such as elastomer polishing body and belt drive, and comparatively many stimulating components, such as motors, belts (natural frequency), robots, various bearings, signs of wear, etc. Therefore initial tests are made on a test rig with a S6001 bearing. The structure of the test rig is shown schematically in Figure 5. The bearing is attached to the test stand with a flange. The inner ring of the bearing rotates while the outer ring remains static. The bearing is loaded radially in the z-axis. The test stand reproduces an idealized state in order to make frequencies visible without interfering elements. The knowledge gained from this can be used for the further experiments.

2.3 Metrology

Two different measurement set-ups are used to measure the vibrations. Due to different objectives two different sensors are used. Both sensors are triaxial accelerometers, where the

Table 1. Basic frequency factors of S6001 bearing.

Units [Hz]	Basic frequency factors related to s^{-1}	Basic frequency factors related to rpm		
RPM	1/60	300	600	1000
BPFFO	3.0476	15.238	30.4760	50.7933
BPFFI	4.9524	24.762	49.5240	82.5400
BSFF	1.9809	9.9045	19.8091	33.0151
RPFFB	3.9618	19.809	39.6182	66.0303
FTFFI	0.3810	1.905	3.8095	6.3492
FTFFO	0.6191	3.0955	6.1905	10.3175

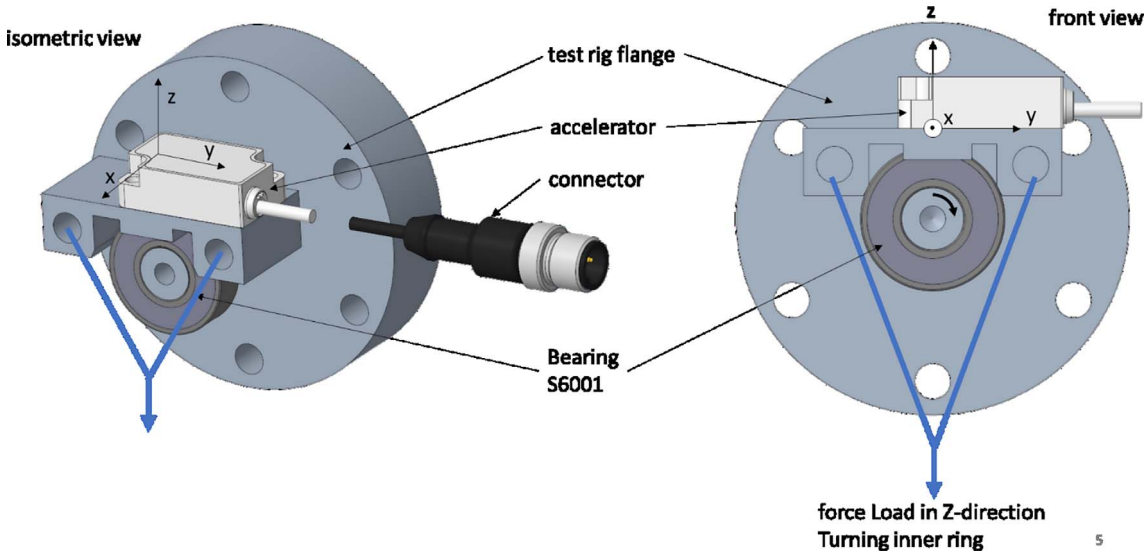

Figure 5. Schematic test rig set up.

main differences can be seen in Table 2. For example, the first measurement set-up is intended for later use in production, while the second test serves to qualify whether the first measurement set-up is sufficient for the requirements of bearing monitoring.

For the first setup, the sensor Balluff BCM0001 [34] is used, which was specially developed for condition monitoring for industrial use. This is an intelligent sensor that has an IO-Link interface. With this type of sensors, the process data recorded by the sensor are processed directly in the sensor and the results from this data processing are transmitted digitally to an IO-Link master. In this setup the IO-Link master AL1060 [35] from the company IFM is used, which can be connected to a computer. Besides the cost-effectiveness, these sensors are really user- and maintenance-friendly, because they are for example very easy to integrate into a new or consisting system and have mostly additional built-in sensors, which can signal a malfunction of the sensor to the user. These advantages make this sensor really suitable for the vibrations analysis of a polishing head in industrial environment. The biggest disadvantage of the Balluff condition monitoring sensor is that due to the low update rate and the necessary pre-processing of the data in the sensor, no comprehensive data analysis can be carried out by the user. For example, only maximum/minimum or averaged values over a large measurement period (here: ~100 ms) can be obtained. Thus, it is not possible to qualify whether the signals obtained are composed of the vibrations caused by the bearings or whether the signal consists of other signals caused by the motor, belt or gear for example. Therefore, for the second measurement chain, the sensor OS-325MF-PG [36] from the company ASC is used, which is an integrated sensor, meaning in this case the measured acceleration values are converted into a normalized electrical signal between (here: ± 10 V). This signal can then be digitised by any ADC operating in this signal range. For this experimental the device NI USB-6001 [37] is used, which is a data acquisition device, which can be controlled by a computer. This measurement system allows to log data at the needed rate of 1400 Hz. This frequency was choosen to fulfil the Nyquist–Shannon-Theorem, because the maximum frequency response of the sensor is 700 Hz. With the logged data, the vibration data can be evaluated in more depth. For this work, a frequency analysis is made, to evaluate if the measured signal is mainly produced by the bearings. If so, the frequency analysis allows to get information about the condition of the bearings (see Chapter 1).

Table 2. Comparison of the two sensors used.

Sensor	Balluff BCM0001	ASC OS-325MF-PG
Sensor type	Intelligent	Integrated
Frequency range	2...3200 Hz	0...700 Hz
Number of measuring axes	3	3
Measuring principle	MEMS	MEMS
Range acceleration vibration	±16 g	±5 g
Data preprocessing	Yes	No
Interface	IO-Link	Analog (±10 V)

Table 3. Design of experiments input parameters and target parameters.

Input parameter	Unit	Lower limit	Upper limit	Target parameter
Force	N	5	25	Root Mean Square (RMS) in the *X*-axis
Rotations per minute	min^{-1}	600	1200	Root Mean Square (RMS) in the *Z*-axis
Runtime	min	5	10	Peak-to-Peak (PtP) in the *X*-axis
Bearing condition	–	New milled-Rusty	New milled-Rusty	Peak-to-Peak (PtP) in the *Z*-axis

2.4 Design of experiment

Experimental design is known to help to precisely understand the relationship between input parameters and target parameters without huge time consuming, without trial and error iterations and with as few experiments as possible. In order to clearly understand the influence of the applied force and the rotation speed during the polishing process on the measured vibrations a Design of Experiment (DOE) was set. With the DOE it is then possible to understand how big are the vibrations variations upon changing the applied force and the rotation speed without making unnecessary trials.

For the generation of DOE the commercial software for statistical experimental design named *Design-Expert* from the company STAT-EASE was used. The parameters applied force (N), rotation speed (min^{-1}), runtime (min) are discrete input parameters. The bearing condition (new, milled, rusty) serve as a nominal input parameter. The target parameters are the output parameters from the Baluff sensor, which in this case are the Root Mean Square (RMS) of two axis and the Peak-to-Peak (PtP) of the same two axis. An optimal custom design was chosen for the generation of the DOE and a total of 25 individual experiments were necessary to complete the DOE. The following Table 3 shows the input parameters, necessary for the generation of the DOE, as well as the target parameters. The generated DOE was conducted in the test rig for the usage of both vibration measuring sensors. The results of the conducted DOE will be discussed in the next chapter.

2.5 Programming

The sensor data of the polishing head, including the vibration sensor data, are evaluated with the Python programming language or used further with Python for machine learning. The latter is used to make statements about the material removal onto the workpiece surface and/or the condition of the polishing head. For this data processing, the data are monitored and stored.

3 Results

3.1 Test rig

In the following subchapter, the results conducted on the test rig using the Baluff intelligent sensor and ASC sensor are presented. The statistical software creates a deterministic model with a prediction accuracy of the vibrations of 34.60% (RMSX, Pearson correlation, R^2). This allows conclusions to be drawn about the accuracy of the process prediction and the influence of the individual parameters. The statistical software cannot accurately represent random scatter and runs behind expectations. Figure 6 shows the results from the conducted DOE, where a correlation is observed between the applied force and rotation speed to the measured vibration. On the left side of Figure 6, it is observed that with the increase of the applied force to the bearing the measured vibration is increased and vice-versa. The same effect occurs when the applied rotation speed of the bearing is increased and the measured vibrations also increase and vice-versa, as shown in the middle of Figure 6.

The software can also assign the bearing conditions to the vibration data. However the bearing conditions in the production environment are target parameters and not input parameters. This means that the bearing condition is an unknown variable and should be determined by means of vibration sensor. The deterministic model can be determined with a prediction accuracy of 99.02%, when the bearing condition is given as an input parameter into the DOE. The right side of Figure 6, shows the correlation between the bearings condition and the measured vibration. It is

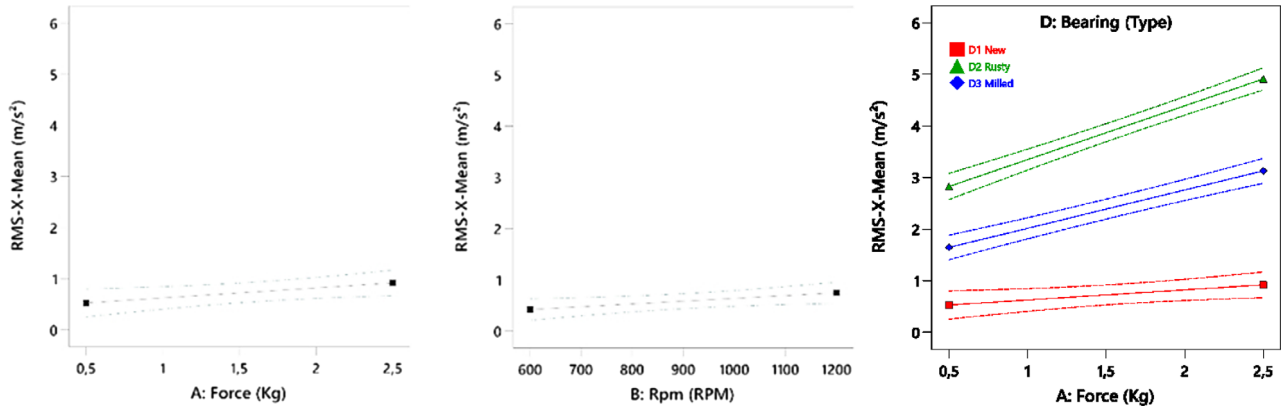

Figure 6. DOE results on the test rig using the Baluff sensor. Left: correlation between the applied force and the measured vibration. Middle: correlation between the applied rotation speed and the measured vibration. Right: correlation of the vibration of each different bearing condition with the applied force.

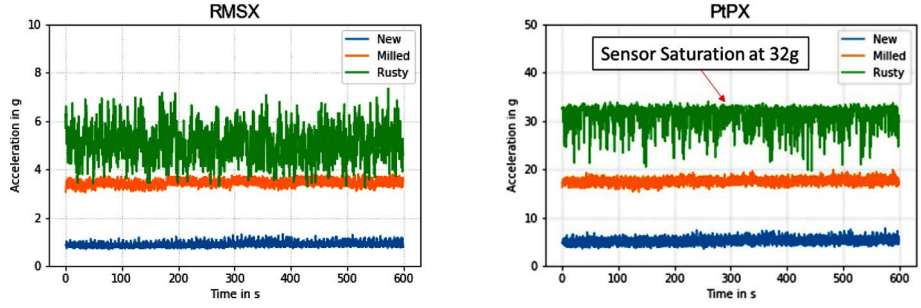

Figure 7. Vibration measurements, using the Baluff sensor, in the axial direction of the three different bearings: new, milled and rusty. Left: Root Mean Square (RMS); Right: Peak-to-Peak (PtP).

seen that vibration sensor can assign the vibration to each different bearing condition.

The following Figure 7 shows the vibration measurements of the conducted DOE, comparing the bearings with three different conditions: new, milled and rusty. It is seen from the figures on the left (RMS) and right side (PtP) that the produced vibrations are different according to the tested bearing. The new bearing (blue curve) show less vibrations compared to the milled bearing and the rusty bearing, for both analysing parameters: RMS and PtP. Vibrations of around 1 g RMS are measured for the new bearing, while vibrations of more than 3 g RMS are measured for the milled bearing and for the rusty bearing approximately between 4 g and 6 g RMS. For the analysing parameter PtP, the new bearing shows vibrations around 5 g, the milled bearing shows almost 20 g and the rusty bearing approximately 31 g hitting the sensor saturation at 32 g.

The following Figure 8 shows the vibration measurement of the four bearings: one new bearing with a runtime of 50 h and three new bearings with a runtime of 0 h. From these results it is seen that the bearing with a runtime of 50 h (blue curve) shows higher deviation in terms of RMS and PtP values compared to the other completely new bearings.

During the experiments conducted in the test rig using the Baluff sensor, different assembling methods were tested: air, beeswax, soup and oil. The goal of this investigation was to check whether the different fluids would cause an impact/damping/transfer of the vibrations from the bearing to the sensor. From the conducted trials no signification differences could be seen between the four different tested assembling methods.

In the following Figure 9, the results conducted on the test rig using the ASC sensor are presented. While the Baluff sensor provides processed data from the raw signal, the ASC provides the raw signal from the vibration measurement of three different axis. The resulting vector from all three axis sensor data was calculated and further used to conduct a Fast-Fourier-Transformation converting the signal from a time spectrum into a frequency spectrum. Figure 9 shows the conducted FFT on the vibration measurement for each different bearing: new, milled and rusty. On one hand, it is observed from the FFT for the new bearing that no frequencies with high intensity are measured. On the other hand, for the FFT of the milled and rusty bearing new frequencies are being measured. Table 1 shows the basic frequencies, meaning the 1st Harmonic frequencies, that are expected to be measured on the S6001 Bearing. If on any of these frequencies a high frequency peak is measured, it is then possible to measure a defect at a specific component of the bearing, according to the measured frequency. For the milled bearing it is observed a frequency peak at approximately 30 Hz, 60 Hz and 90 Hz. These values correspond to the 1st, 2nd

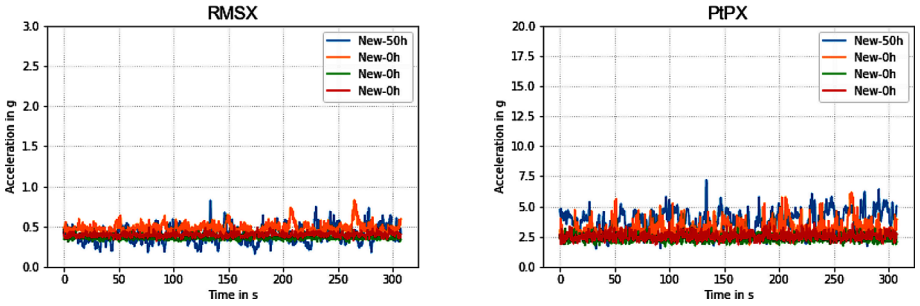

Figure 8. Vibration measurements, using the Baluff sensor, in the axial direction of four bearings with different conditions: new 50 h runtime and new 0 h runtime. Left: Root Mean Square (RMS); Right: Peak-to-Peak (PtP).

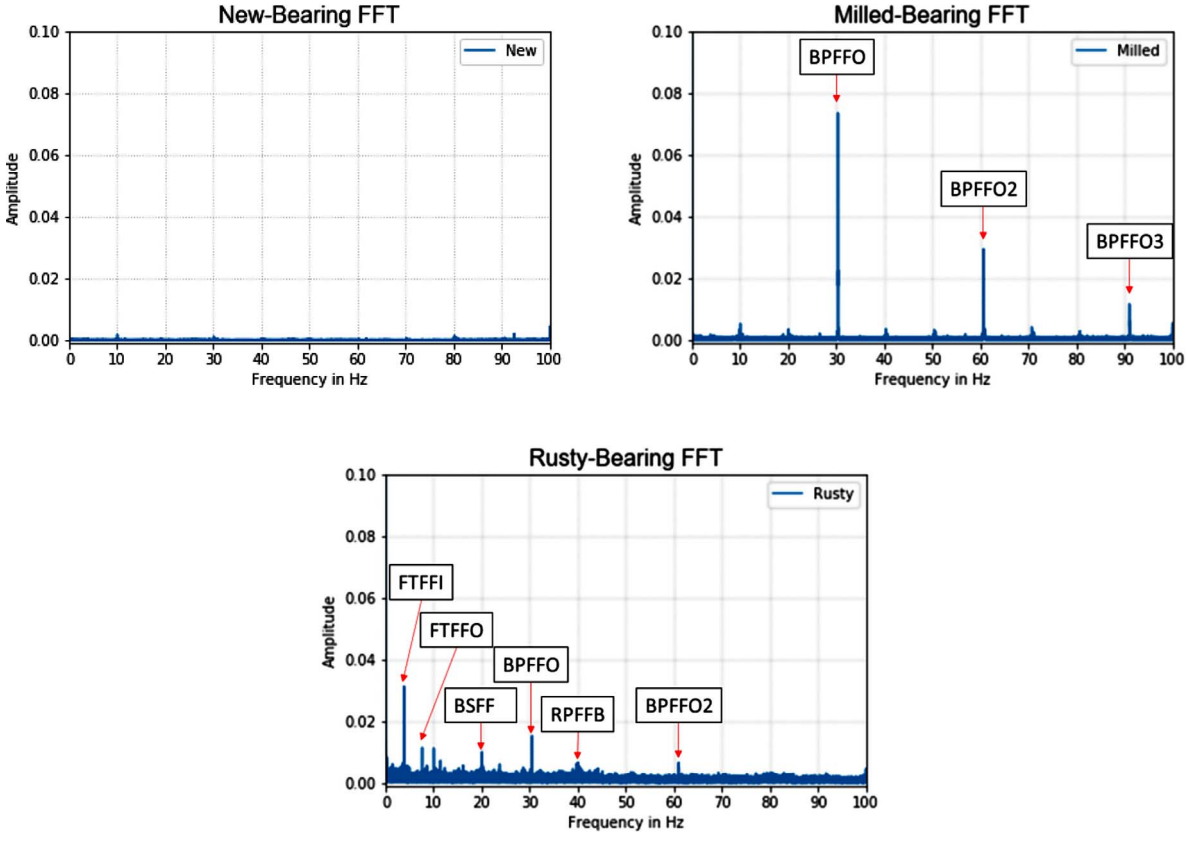

Figure 9. Vibration measurement, using the ASC sensor, of three different bearings: new, milled and rusty.

and 3rd Harmonic of the Ball Pass Frequency Factor Outer (BPFFO) for a rotation speed of 600 rpm. From this diagram it is observed and proven that the defect on the outer ring of the bearing could be measured by the ASC sensor. For the rusty bearing more frequencies are observed. The 1st and 2nd Harmonic frequencies (30 Hz and 60 Hz) of the BPFFO are also measurable on the rusty bearing. At a frequency of 20 Hz a peak is observed, which corresponds to the Ball Spin Frequency Factor (BSFF). The same happens for the frequency 40 Hz, where a small peak is measured for the Ring Pass Frequency Factor on Rolling Element (RPFFB). As last, frequencies of approximately 4 Hz and 6 Hz are measured that correspond to the Fundamental Train Frequency Factor Inner (FTFFI) and Outer (FTFFO) respectively. The rotational speed is 600 rpm or 10 s^{-1}, which is also visible in the frequency by the peak at 10 Hz.

3.2 Polishing head

In the following subchapter, the results conducted on the polishing head using Baluff intelligent sensor and the ASC sensor are presented. Since there are much more vibrations with the robot and the polishing head compared with the test rig, during some trials with 600 rpm and 1200 rpm the saturation of the ASC sensor was achieved. For this reason the rotation speed was adjusted to 300 rpm for all of the following presented results.

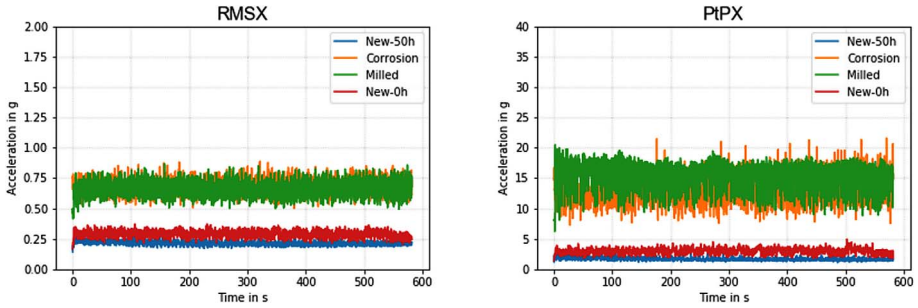

Figure 10. Vibration measurements of the four bearings with different status (new 50 h, corrosion, milled and new 0 h) bearings measured in the axial direction during the polishing head trials. Left: Root Mean Square (RMS); Right: Peak-to-Peak (PtP).

In the beginning the Baluff sensor was tested in order to see if it would be possible to see the different bearing conditions in the polishing head, reproducing the same results shown in Figure 7. The following Figure 10 shows the vibrations measurements conducted in the polishing head, when different bearing states were used: new, milled and rusty. It is seen that the condition of the bearings during the conducted trials could be monitored and associated with the respective bearing status. The new bearing (red curve) and the new bearing 50 h (red curve) show less vibrations compared with the milled bearing (green curve) and the rusty bearing (orange curve). The new bearings shows vibrations around 0.25 g RMS while the milled bearing and the rusty bearing show vibrations around 0.6 g RMS. In terms of PtP the new bearings are approximately at 3 g and the milled bearing and the rusty bearing at around 15 g. It can be concluded that with the Baluff intelligent sensor extreme different bearing condition can also be monitored during the robot polishing process.

For the ASC sensor, the goal was to obtain also similar results as during the tests in the test rig. The aim was to also detect the individual frequencies of the bearings as shown in Figure 9, and detect the damages in the individual components of the bearings. For the analysis of these results the measurements of the three different axis were taken into consideration and the resulting vector was calculated as in the previous results conducted in the test rig. Afterwards a FFT was conducted to convert the signal into a frequency spectrum. Since there are a lot of more frequencies during the trials on the polishing head, overlapping each other, it is hard to take any conclusions from entire frequency spectrum. For this reason, the invidual frequencies were analysed.

Before comparing the individual single frequencies, it is important to explain that the reproducibility of the rotation speed of the polishing head was not always the same. The following Figure 11 shows the frequency of the rotation speed of the motor, which was set at 300 rpm, meaning at 5 Hz. It is seen that this frequency has a little offset from trial to trial and that the amplitudes are also different. For the new bearing a higher amplitude is observed compared with the rusty and the milled bearing. This has an influence in the upcoming results since this frequency reproduces itself on its following harmonic frequencies making the difference between bearings less visible.

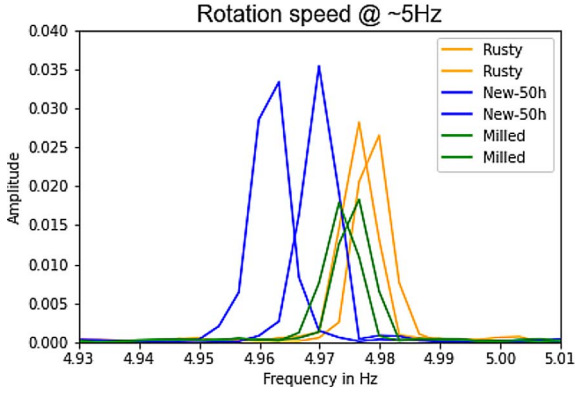

Figure 11. FFT of the conducted trials on the polishing head at 5 Hz.

With this being said, the following Figure 12 shows the six basic frequencies of the bearings for three different status: new 50 h, Milled and Rusty. It was expected for the rusty bearing to have higher amplitude on almost all basic frequencies and for the milled-bearing to show a higher amplitude for the BPFFO (outer ring damage) compared to the new bearing. It is seen that for all the frequencies, expect for the RPFFB, the rusty bearing shows higher amplitudes compared to the new bearing. This means that the damage of the bearing can be detected on its individual components during the robot polishing process. It is also seen that the milled bearing for the BPFFO frequency does not show the high amplitude that it was expected due to the high damage on the outer ring. The reason behind this may be due to the fact that the force applied by the polishing head on the bearing was conducted axially and not radially. If the force would have been radially, as in the test rig, the bearing balls would be pressed into the milled groove producing a higher amplitude on this frequency.

4 Discussion

Vibrations play a major role in polishing: on the one hand, they lead to a supply of polishing agent in the effective area and to an increase in mechanical removal, but on the other hand, they also lead to local temperature increases, contact between the optics and the polishing tool and to a

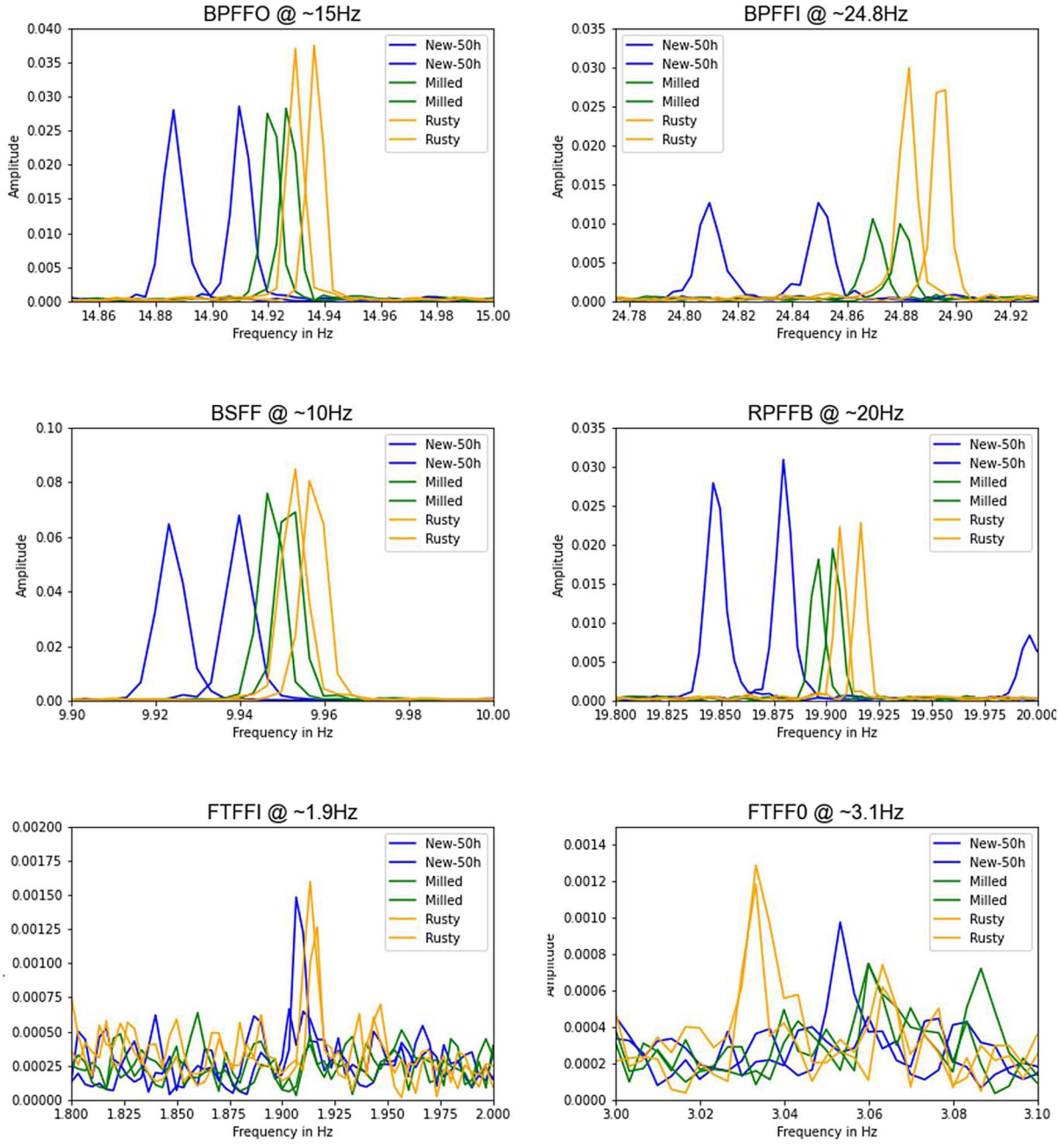

Figure 12. FFT of the conducted trials on the polishing head, showing the different basic frequencies (BPFFO, BPFFI, BSFF, RPFFB, FTFFI, FTFFO) of the three tested bearings.

fluctuation in force. Depending on the intensity of the frequencies, the material removal can be increased and the roughness can be improved by minimising the frequencies.

For vibration sensors, the mounting of the sensors plays a significant role: the air gap between the sensor and the mounting surface must be eliminated. Preliminary tests have shown that screwing on and using grease or oil in the air gap is suitable. In the field of vibration measurement, beeswax, glue or magnets are also used.

At the beginning, frequency analyses were carried out on a test rig to exclude interfering elements. A DOE was created to generate a parameter selection and a test sequence. In comparison to the speed, the influence on the force is more significant. Already in the statistical evaluation of the data, a distinction can be made between the bearing conditions new, rusted and with damage on the running surface. The rusted bearing simulates a grease-free bearing with increased bearing play due to wear. The differentiation of the states can take place in real time in the process without previous training etc. and no machine learning or big data is necessary for this.

A distinction can be made with both sensors. It is worth noting that the Balluff sensor allows fewer conclusions to be drawn about the bearing frequencies, but is much more

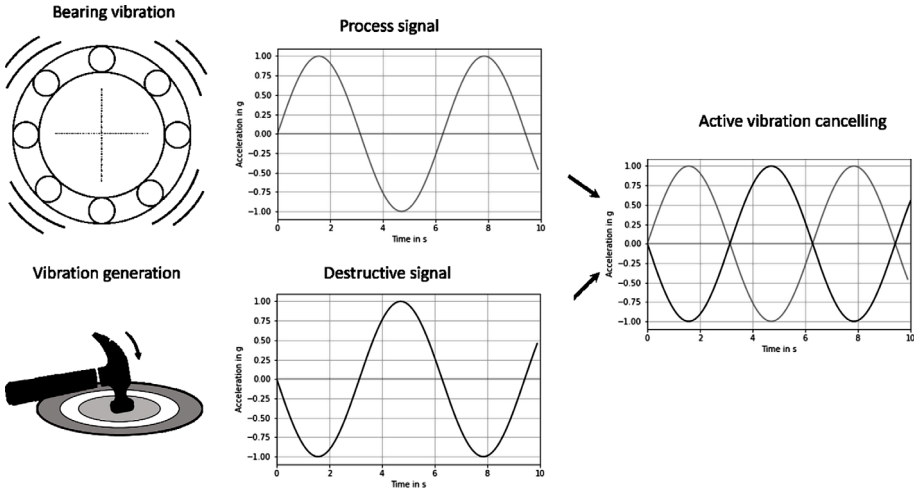

Figure 13. Schematic illustration of the process vibrations and a possible frequency shift with a counter signal for cancellation, that works as Active Vibration Controlling.

economical and provides a simple plug-and-play solution through the use of IO-Link. The intelligent sensor processes the data already during recording and therefore does not allow any conclusions to be drawn about the raw data and thus the individual sensor data introduced. The results are validated in several tests for repeatability.

Figure 10 suggests, however, that the bearings must first run in on the polishing head, as bearings with a running time of 50 h have lower frequencies. A bearing with 50 h was used, as there it can be assumed that the bearing has run in. The bearing manufacturer SKF specifies a running-in time of at least 48 h [38]. Here, it would make sense to consider separately and retrospectively from when a bearing is run in and from when it is worn out. Figure 8 shows that the repeatability of the frequencies of the brand new bearing cannot be guaranteed. Running in the bearing allows a detailed prediction of these frequencies. This leads to a limited running time and to a change in machining: after run in of the bearing the optic will be later polished with the pre conditioned bearing.

Sensor data can even be used to determine where the damage is located: Inner or outer ring or on the rolling elements, in the latter case even exactly which rolling element.

Since the frequencies of a polishing head can be measured on the surface of the optics and these are demonstrably due to the rolling bearings, it is advisable to use aerostatic bearings or hydrostatic bearings. The virtually non-existent wear on these bearings will also result in longer service lives. Vibrations should not be completely avoided in the process. Only disturbance frequencies and wear vibrations should be avoided or eliminated. Such vibrations are also helpful in supplying polishing suspension in the polishing gap.

5 Summary and outlook

The polishing of glass, glass ceramic and ceramic components will play an increasingly important role in the production of high-precision parts in the future. Due to the many process parameters in the polishing process and their insufficient research, the process is not as stable as comparable mechanical material removal processes. One of these hardly considered fields of research are vibrations and bearings in the polishing process. Bearings are subject to wear with increasing running time and generate six frequencies plus their respective multiples. The bearing frequencies are clearly visible in the vibration sensor data for a worn bearing and a damaged bearing. It is assumed that these frequencies are also visible on the glass surface after polishing. With increasing wear or damage, the frequencies also increase accordingly.

In this publication it was shown that the bearing frequencies influence the polishing tool and can be measured. The individual bearing frequencies are not visible with new bearings, but become increasingly visible with increasing damage (worn, damage on the running surface or rust). Statements can even be made about which surface (outer or inner surface, cage or which rolling element) the damage is on.

A correlation between the polishing force normal to the surface and the vibrations could be shown. With increasing damage, the process divergence increases and thus the deviation from the target.

Some precautions need to be taken for the future and any recommendations are addressed below: In order to reduce disturbance frequencies of the bearings or their wear, there is the possibility to replace the bearings with main influence. There is a choice of magnetic or aerostatic bearings or flexure hinges. Magnetic and aerostatic bearings are more cost-intensive and require more maintenance than conventional roller bearings, but have a higher efficiency and hardly any wear or interference frequencies. Another option on the eccentric is to use a flexure hinge as a bearing. Flexure hinges have only material friction and can also be operated without problems below the polishing slurry liquid level. The disadvantage is the large construction and the cost-intensive manufacturing [39].

Another possibility for reducing the individual interference frequencies is the use of Active Vibration Controlling (AVC). Based on the measured vibration, the same frequency with a phase shift is created and coupled into the component. This results in destructive interference and both vibrations extinguish themselves (schematic view: Fig. 13). Nowadays, this is possible thanks to high-performance calculations and powerful computers. There are a number of different electrical circuits, each of which follows the principle of phase shifting the voltage of the vibration sensor by almost 90° in order to drive a piezo transducer. This is called a gyrator circuit. Various methods can be used as actuators, as follows:

- Piezoelectric effect: the application of an electrical voltage results in the change in length of a material (e.g. α-quartz SiO_2) [40].
- Magnetostrictive effect: the application of a magnetic field leads to a change in the length of a material (e.g. Permendur $Fe_{49}Co_{49}V_2$) [41].

Similar thermal or fluid-based systems are only suitable for passive damping due to the system inertia. Because of the measurement of the vibration, an acceleration sensor is already present, so that part of the setup for AVC is already in place. Such an approach is already being used in automotive (example: exhaust technology) [42], for 3D printers [42], measuring equipment [43], etc. By using such systems, the frequencies can be shifted into a range that is no longer relevant for the application. This is of particular interest for EUV lithography.

The vibration generated by the polishing head is constant because of the constant speed during polishing. AVC, which involves offsetting a frequency with its counterfrequency requires to generate the corresponding counterfrequency. The actual frequency can also be recorded in real time via an air or structure-borne sound microphone directly at the polishing head. The recorded acoustic signal can then be analysed with software (for example python package *librosa* [44]) and a phase-shifted signal can be output to a structure-borne sound microphone. This process also achieves Active Vibration Controlling.

In the future, the path will be towards more controlled process fluctuations, but this also means in terms of vibrations: Solid state joints, air bearing spindle and AVC. The latter for the remaining process vibrations.

Competing interest

The authors declare that they have no competing interests.

Funding

The work is part of a funded German research project named OpTec 4.0 with the goal of funding young scientist, contract number 13FH003IB6. The authors would like to thank the Federal Ministry of Education and Research for funding this project.

Availability of data and materials

The datasets used and/or analysed during the current study are available from the corresponding author on reasonable request.

Author's contributions

MS has the initial idea of this research topic. He designed all necessary CAD models, and take the decision of using a test rig for initial tests. MS was a major contributor in writing the manuscript. RA has managed the whole project (time slots at the test rig, and at the robot polishing station), and was a major contributor in analyzing the data sets. SV has qualified and selected the sensor types. He also wrote the sections of that topic in this publications. His knowledgement about vibrations made the project first possible. IB executed the DoE and generated the results. RB supervised the whole project and arranged the financial stuff for this publication. All authors read and approved the final manuscript.

Acknowledgments. We would especially like to thank the Faculty of Mechanical Engineering at Aalen University, especially Prof. Markus Kley, Manuel Bauer and Julia Weidenauer for their support.

References

1 Preston F.W. (09.02.1922) The structure of abraded glass surfaces, *Trans. Opt. Soc.* **23**, 141.
2 Cook L.M. (1990) Chemical processes in glass polishing, *J. Non-Cryst. Solids* **120**, 1–3, 152–171.
3 Evans C.J., Paul E., Dornfeld David, Lucca D.A., Byrne G., Tricard M., Klocke F., Dambon O., Mullany B.A. (2003) *Material removal mechanisms in lapping and polishing*, Laboratory for Manufacturing and Sustainability, UC Berkeley. https://escholarship.org/uc/item/4hw2r7qc.
4 Klocke F., Zunke R. (2009) Removal mechanisms in polishing of silicon based advanced ceramics, *CIRP Ann.* **58**, 1, 491–494.
5 Klocke F., Brecher C., Zunke R., Tuecks R. (2011) Corrective polishing of complex ceramics geometries, *Precis. Eng.* **35**, 2, 258–261.
6 Becker E. (2011) *Chemisch-mechanische Politur von optischen Glaslinsen (Berichte aus der Werkstofftechnik)*, Zugl.: Aachen, Techn. Hochsch., Diss., Shaker, Aachen.
7 Lee H., Lee D., Jeong H. (2016) Mechanical aspects of the chemical mechanical polishing process: a review, *Int. J. Precis. Eng. Manuf.* **17**, 4, 525–536.
8 Brecher C., Esser M., Witt S. (2009) Interaction of manufacturing process and machine tool, *CIRP Ann.* **58**, 2, 588–607.
9 Brinkmann U. (ed.) (2000) *Deutsche Agenda Optische Technologien für das 21. Jahrhundert: Potenziale, Trends und Erfordernisse*, VDI-Technologiezentrum, Düsseldorf.
10 Ghosh G., Sidpara A., Bandyopadhyay P.P. (2018) *Fabrication of optical components by ultraprecision finishing processes*, Springer Link, pp. 87–119.
11 National Research Council (1999) *Harnessing light: optical science and engineering for the 21st century*, 2 print ed., National Acad. Press, Washington.

12 Mullany B., Mainuddin M. (2012) The influence of process vibrations on precision polishing metrics, *CIRP Ann.* **61**, 1, 555–558.
13 Cooke F. (1976) Optical activities in industry, *Appl. Opt.* **15**, 2, 293.
14 Saruhan H., Sandemir S., Çiçek A., Uygur I. (2014) Vibration analysis of rolling element bearings defects, *J. Appl. Res. Technol.* **12**, 3, 384–395.
15 Kojima T., Miyajima M., Akaboshi F., Yogo T., Ishimoto S. (1999) Practical use of CMP process monitor in Cu polishing, in: *1999 IEEE international symposium on semiconductor manufacturing conference proceedings (Cat No. 99CH36314)*, IEEE, pp. 187–190.
16 Rao P.K., Bhushan M.B., Bukkapatnam S.S.T., Kong Z., Byalal S., Beyca O.F. Fields A., Komanduri R. (2014) Process-machine interaction (PMI) modeling and monitoring of chemical mechanical planarization (CMP) process using wireless vibration sensors, *IEEE Trans. Semicond. Manuf.* **27**, 1, 1–15.
17 Hetherington D.L., Stein D.J., Lauffer J.P., Wyckoff E.E., Shingledecker D.M. (1999) Analysis of in-situ vibration monitoring for end-point detection of CMP planarization processes, in: Amberiadis K., Kissinger G., Okumura K., Pabbisetty S., Weiland L.H. (eds.) *In-line characterization, yield reliability, and failure analyses in microelectronic manufacturing*, SPIE (SPIE Proceedings), p. 89.
18 Reichling M., Gogoll S., Stenzel E., Johansen H., Huisinga M., Matthias E. (1995) Laser damage processes in cleaved and polished CaF_2 at 248 nm, in: Bennett H.E., Guenther A. H., Kozlowski M.R., Newnam B.E., Soileau M.J. (eds.) *27th annual boulder damage symposium: laser-induced damage in optical materials: 1995*, SPIE (SPIE Proceedings), p. 260.
19 Akbari J., Borzoie H., Mamduhi M.H. (2008) Study on ultrasonic vibration effects on grinding process of alumina ceramic (Al_2O_3), *Eng. Technol.* **41**, 785–789.
20 Jianhua Z., Yan Z., Shuo Z., Fuqiang T., Lanshen G., Ruizhen D. (2014) Study on effect of ultrasonic vibration on grinding force and surface quality in ultrasonic assisted micro end grinding of silica glass, *Shock. Vib.* **4**, 1–10.
21 Schopf C., Rascher R., Sperber P. (2010) Vor- und Nachteile der Ultraschalltechnologie beim Schleifen von optischen Flächen, *Achtes Symposium – Zukunft Glas – von der Tradition zum High-Tech-Produkt*, Zwiesel.
22 Bliedtner J., Henkel S., Schwager A., Götze K., Gerhardt M., Fuhr M. (2018) New process chain for the production of complex freeforms, *Opt. Photon.* **13**, 2, 35–39.
23 Ding K., Fu Yucan, Su H., Gong X., Wu K. (2014) Wear of diamond grinding wheel in ultrasonic vibration-assisted grinding of silicon carbide, *Int. J. Adv. Manuf. Technol.* **71**, 9–12, 1929–1938.
24 Suzuki H., Hamada S., Okino T., Kondo M., Yamagata Y., Higuchi T. (2010) Ultraprecision finishing of micro-aspheric surface by ultrasonic two-axis vibration assisted polishing, *CIRP Ann.* **59**, 1, 347–350.
25 Xu W., Lu X., Pan G., Lei Y., Luo J. (2011) Effects of the ultrasonic flexural vibration on the interaction between the abrasive particles; pad and sapphire substrate during chemical mechanical polishing (CMP), *Appl. Surf. Sci.* **257**, 7, 2905–2911.
26 Wolf S. (2002) Deep-submicron process technology, in: Wolf S., Tauber R.N., *Silicon processing for the VLSI era*, vol. **4**, Lattice Press, Sunset Beach, CA.
27 Luo J., Dornfeld D.A. (2004) *Integrated modeling of chemical mechanical planarization for sub-micron IC fabrication: from particle scale to feature, die and wafer scales*, Springer, Berlin, Heidelberg.
28 Mullany B., Byrne G. (2003) The effect of slurry viscosity on chemical–mechanical polishing of silicon wafers, *J. Mater. Process. Technol.* **132**, 1–3, 28–34.
29 Boning D.S., Moyne W.P., Smith T.H., Moyne J., Telfeyan R., Hurwitz A., Shellman S., Tayor J. (1996) Run by run control of chemical-mechanical polishing, *IEEE Trans. Compon. Packaging Manuf. Technol.* **19**, 4, 307–314.
30 SIGENIC (2020) *Sigenic – engineering intelligent solutions: vibration sensor series*. https://www.sigenic.com, accessed 2020-10-26.
31 FAG (ed.) (2019) *Wälzlagerpraxis: handbuch zur gestaltung und berechnung von wälzlagerungen*, Vereinigte Fachverlage GmbH, 5. aktualisierte Auflage. Mainz. (Antriebstechnik)
32 Midpoint Bearing (2021) *Bearing frequencies: formulas to calculate bearing frequencies*, https://www.midpointbearing.com/wp-content/uploads/2017/02/NTN-Bearing-Frequencies.pdf, accessed 2021-12-05.
33 Fernandez F. (2021) *Typical bearing defects and spectral identification*, https://power-mi.com/content/typical-bearing-defects-and-spectral-identification, accessed 2021-12-05.
34 Balluff GmbH(2021) *Condition monitoring sensor with integrated data preprocessing*, Neuhausen. https://www.balluff.com/local/de/products/product-news-overview/product-news/condition-monitoring-sensor/.
35 IFM electronic GmbH (2021) *IO-link master with USB interface: AL1060*. https://www.ifm.com/de/de/product/AL1060?tab=documents.
36 ASC GmbH (20.05.2021) *MEMS capacitive accelerometer: ASC OS-325MF-PG*, Pfaffenhofen. https://www.asc-sensors.de/sensoren/asc-os-325mf-pg/.
37 National Instruments (2014) NI USB-6001: specifications. https://www.ni.com/de-de/shop/hardware/products/multifunction-io-device.html?modelId=124894.
38 SKF (2021) *Nachschmierung und Einlaufen*, https://www.skf.com/de/products/rolling-bearings/engineered-products/high-temperature-bearings-and-bearing-units/relubrication-and-running-in, accessed 2021-12-05.
39 Krause W. (ed) (2018) *Konstruktionselemente der Feinmechanik* 4, vollständig überarbeitete und, Carl Hanser Verlag GmbH & Co. KG, München. (Hanser eLibrary).
40 Hamed Y.S., Kandil A., Machado J.T. (2020) Utilizing macro fiber composite to control rotating blade vibrations, *Symmetry* **12**, 12, 1984.
41 Guo J., Suzuki H., Higuchi T. (2013) Development of micro polishing system using a magnetostrictive vibrating polisher, *Precis. Eng.* **37**, 1, 81–87.
42 Krüger J., Buganza F., Koch V. (2016) The effects of future noise limit values on the design of exhaust systems, *ATZ worldwide* **118**, 9, 48–51.
43 Greco D., Blanc P., Aubry E., Vaclavik I. (2007) Active vibration control of flexible materials found within printing machines, *J. Sound Vib.* **300**, 3–5, 831–846.
44 McFee B., Metsai A. et al. (2021) *Librosa/librosa: 0.8.1rc2*, Zenodo.